

## Simulations of Material Damage to Divertor and First Wall Armour under ITER Transient Loads by Modelling and Experiments

B. Bazylev 1), G. Janeschitz 2), I. Landman 1), S. Pestchanyi 1), A. Loarte 3), G. Federici 4), M. Merola 3), J. Linke 5), T. Hirai 5), A. Zhitlukhin 6), V. Podkovyrov 6), N. Klimov 6), V. Safronov 6), I. Garkusha 7), V. Makhlay 7)

1) Forschungszentrum Karlsruhe, IHM, P.O. Box 3640, 76021 Karlsruhe, Germany

2) Forschungszentrum Karlsruhe, Fusion, P.O. Box 3640, 76021 Karlsruhe, Germany

3) ITER Organisation, Cadarache, Building 523, 13108, Saint Paul Lez Durance Cedex, France

4) EFDA Close Support Unit Garching, Boltmannstr.2, D-85748 Garching bei München, Germany

5) Association Euratom- Institut für Plasmaphysik Jülich, D-5245 Jülich, Germany

6) SRC RF TRINITI, Troitsk, 142190, Moscow Region, Russia

7) Institute of Plasma Physics, Kharkov Institute of Physics and Technology, Kharkov, Ukraine

E-mail of main author: bazylev@ihm.fzk.de

**Abstract.** CFC and tungsten macrobrush armour are foreseen as plasma facing components (PFC) for ITER divertor. Operation of ITER at high fusion gain is assumed to be the H-mode. PFC components manufactured according to the EU specifications for the ITER divertor targets, have been exposed to ITER ELM-like and disruption-like loads at plasma gun facilities in TRINITI. The measured material erosion data was used to validate the numerical simulation codes developed in FZK, which are then applied to model the erosion of the PFCs under the expected loads in ITER. Numerical simulations performed for the expected ITER-like loads predicted: a significant erosion of the CFC target for  $Q > 0.5 \text{ MJ/m}^2$  was caused by the inhomogeneous structure of the CFC; the W macrobrush structure is effective in preventing gross melt layer displacement. Different mechanisms of melt splashing are compared with results obtained in QSPA experiments. Optimization of macrobrush geometry to minimize melt splashing is done. The crack formation at W surface was modelled using the code PEGASUS and validated against the experiments. Simulations carried out for Be armour demonstrated that the Lorentz force generates the violent melt motion thus becoming the most dangerous cause of melt splashing.

### 1. Introduction

The operation of ITER is assumed as the H-mode regime [1] with the transient release of confined plasma energy onto plasma facing components (PFCs) by multiple ELMs and disruptions, which may mainly determine the erosion rate and the lifetime of PFCs [2]. During one ITER discharge about  $10^4$  ELMs are expected. Similarly, disruption power fluxes can affect significantly the PFC lifetime [3]. During ITER operation several hundred disruptions interspaced by ELMs may occur. Plasma energy released in the transients is deposited onto the vessel main wall and the divertor. The expected transient fluxes on the ITER PFCs are estimated in [3,4] as follows. I) Divertor target: Type I ELM heat flux  $0.5 - 4 \text{ MJ/m}^2$  in timescales of 0.3-0.6 ms. Thermal quench heat flux  $2 - 13 \text{ MJ/m}^2$  in 1-3 ms. II) Main wall: Type I ELM heat flux  $0.5 - 2 \text{ MJ/m}^2$  in 0.3-0.6 ms. Thermal quench heat flux  $0.5 - 5 \text{ MJ/m}^2$  in 1-3 ms. Mitigated disruption radiative load  $0.1 - 2 \text{ MJ/m}^2$  in 0.2- 1 ms.

The CFC and tungsten macrobrush armour as the PFC for ITER divertor and the dome, and beryllium large scale macrobrushes for the first wall (FW) armour are foreseen. During the intense transient events in ITER surface evaporation (CFC, W, Be) and surface melting (W, Be) are seen as the main mechanisms of PFC erosion. The melt motion in a thin layer of metallic armour may produce surface roughness, droplet splashing and thus dust emission in form of solidified droplets. Due to a rather anisotropic thermal conductivity of CFC fibres, a noticeable erosion of PAN fibres was observed in experiments at the plasma gun facility QSPA-T [5;6]. Cracks formation in the CFC armour leads to a significant decrease of thermal conductivity and the brittle destruction (BD) results in intense dust production. A rather

intense crack formation was observed at the QSPA-T also for the W targets under rather moderate plasma heat loads [5-7].

The expected erosion of ITER PFCs under the transient loads can be adequately estimated by numerical simulations using the codes validated against the target erosion data obtained in the experiments at the plasma gun facilities QSPA-T, MK-200UG and QSPA-Kh50. Within a collaboration established between EU fusion programme and RF (TRINITY and the Kurchatov Institute) CFC and W macrobrush targets manufactured for the ITER divertor, have been exposed to ITER ELM-like and disruption-like loads in the range 0.5-2.5 MJ/m<sup>2</sup> with the pulse duration of 0.5 ms at the plasma gun facilities at TRINITY [5;6]. The measured material erosion has been used to validate the modelling codes, PEGASUS, MEMOS, PHERMOBRID and FOREV that have been then applied to model the erosion of the divertor and main chamber ITER PFCs under the anticipated transient loads. In frame of the material damage simulations the code FOREV [8] was applied for calculation of parameters of the plasma shield formed from evaporated material in front of the target, for expansion of eroded material into the SOL, and for estimation of radiation heat loads at FW. FOREV data were used by the MEMOS for the erosion estimation of divertor and FW PFCs.

The code MEMOS describes two-dimensional and three dimensional melt processes. The melt motion is described with taking into account the surface tension, the viscosity of molten metal, and the radiative losses from hot tungsten surface. The plasma pressure variations along the divertor plate, as well as the gradient of surface tension and the Lorentz force of the currents crossing the melt layer immersed in strong magnetic field, produce the melt acceleration. In addition the melt splashing generated by growth of surface waves due to the Kelvin-Helmholtz instability and the Rayleigh-Taylor instability is implemented.

The numerical simulations performed for Be armour demonstrated that the Lorentz force generates the violent melt motion and this force becomes the most dangerous mechanism of the melt splashing for the FW. The radiation loads at the FW armour that appear during mitigated disruption can lead to strong damages, such as the melting of whole FW surface up to the thickness of hundreds microns.

The CFC brittle destruction erosion was calculated applying the three-dimensional codes PHERMOBRID and PEGASUS in which thermal conductivity of CFC matrix degradation due to the crack formation is taken into account. The numerical simulations performed for the expected in ITER transient energy density  $Q = 0.5-3.5 \text{ MJ/m}^2$  (ELMs) and  $Q > 5 \text{ MJ/m}^2$  (disruptions) for CFC and W armours [9] demonstrated that significant erosion of the CFC target starts at the loads above  $\sim 0.5 \text{ MJ/m}^2$ . On the other hand, the W macrobrush structure is effective in preventing gross melt layer displacement during ITER ELM-like loads leading to decreasing overall erosion of W at those conditions. To minimize melt splashing caused by the Rayleigh-Taylor instability and total erosion under ITER-like transient loads, an optimization of macrobrush geometry was done [9,10]. The mentioned mechanisms of melt splashing are compared with the results obtained in dedicated experiments at the QSPA-T facility [11]. In addition, for Be and W armour the influence of ELM shape on the melting and evaporation thresholds was numerically investigated [12].

Experimental investigation of surface degradation of bulk tungsten target under repetitive ELM-like heat loads have been performed at QSPA facility in Kharkov Institute of Plasma Physics [13;14]. Crack formation at the W surface was modelled, using the code PEGASUS, and a reasonable agreement with the experimental data of QSPA-T [7] and QSPA-Kh50 [14]

facilities has been obtained. Simulations of carbon dust production have been performed, also using the PEGASUS validated against the experimental data on the MPG-8 graphite and the CFC erosion rates measured at the MK-200UG facility. After the validation the PEGASUS simulations reproduced main morphology features of eroded surface of graphite and the sizes of debris, as well as the measured erosion rate.

## 2. Experimental results on CFC and W brush erosion:

**Experiment.** The targets consisted of separate tungsten and CFC elements of sizes  $9.5 \times 9.5 \times 3 \text{ mm}^3$  and  $19.5 \times 19.5 \times 3 \text{ mm}^3$  brazed to a supporting stainless steel plate with 0.5 mm gaps between brushes was exposed to series of repeated plasma pulses (100 in each series) with energy density in a range of 0.5-2.5  $\text{MJ/m}^2$  and 0.5 ms duration. The target was preheating up to  $500^\circ\text{C}$ . The plasma stream has Gaussian profile with half width of 8 cm and was inclined under angle of  $30^\circ$  to the target surface. The plasma pressure varied in range of 0.3 – 0.9 MPa. After every pulse (for  $Q > 2.5 \text{ MJ/m}^2$ ) and after each series of 10-20 pulses for ( $Q < 1.5 \text{ MJ/m}^2$ ) the target was investigated: a) the target was weighted to determine the mass loss and the average erosion value, b) the surface was inspected by means of the scan electron (SEM) and optical microscopes. Most important results on damage of CFC and W castellated targets under ELM-like heat load ( $Q = 0.5\text{-}1.5 \text{ MJ/m}^2$  and 0.5 ms duration) was described in [5] and presented at IAEA FEC21. Here the new results are presented.

### 2.1. Erosion of CFC macrobrushes

The CFC castellated target was exposed by 5 plasma pulses at the energy density  $Q > 2.2 \text{ MJ/m}^2$ , and the plasma pulse duration of 0.5 ms. After 5 pulses during post-mortem characterizations in FZJ, the surface profile of the target was measured by a laser profilometer to find the value of material losses.

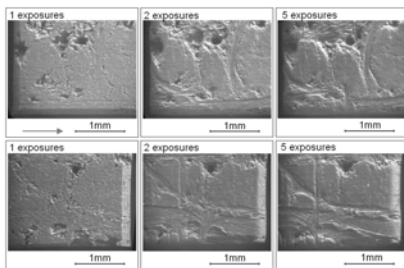


FIG 1 The view of the CFC tile surface obtained by means of electron microscope.  $Q > 2.2 \text{ MJ/m}^2$

The PAN-fiber erosion value, obtained by optical measurements, equals to  $6 \mu\text{m/pulse}$ , but the average erosion value of the sample defined by mass loss measurements equal to  $3 \mu\text{m/pulse}$ . This result indicates that PAN fiber damage is a main erosion mechanism of CFC samples. The Scan electron microscopy investigation confirms this point (See Fig. 1) because the significant erosion of PAN fibers

was observed already after second shot. As a result of disruption-like experiments and ELM-like experiments [5] the CFC macrobrush samples erosion can be characterized by following way:  $Q < 0.5 \text{ MJ/m}^2$  – negligible erosion;  $0.5 < Q < 0.6 \text{ MJ/m}^2$  erosion of the plasma facing edges of brushes;  $0.6 < Q < 0.9 \text{ MJ/m}^2$  erosion of PAN fibres at the plasma facing edges of brushes and at the brush surface after 100 pulses;  $0.9 < Q < 1.3 \text{ MJ/m}^2$  noticeable erosion of PAN fibres after 50 pulses;  $1.3 < Q < 1.4 \text{ MJ/m}^2$  significant erosion of PAN fibres after 10 pulses, erosion of PAN-fibers exceed  $2 \mu\text{m}$  per pulse;  $Q > 2.2 \text{ MJ/m}^2$  significant erosion of PAN fibres after first pulses, erosion of PAN-fibers exceed  $6 \mu\text{m}$  per pulse.

### 2.2. Erosion of pure and lanthanum tungsten macrobrushes.

Two lanthanum tungsten castellated targets were exposed by 100 plasma pulses at the energy density 0.5 and  $1.0 \text{ MJ/m}^2$ . The third lanthanum tungsten castellated target was exposed by 5 plasma pulses at the energy density more than  $2.2 \text{ MJ/m}^2$ .

The result of analysis of the data obtained in these experiments with accounting the results of ELM experiments [5] the W macrobrush samples erosion can be characterized as:

**Table 1**

	W (>99,96%), (Q, MJ/m <sup>2</sup> )	W-1%La <sub>2</sub> O <sub>3</sub> (Q, MJ/m <sup>2</sup> )
Edges melting	>0.4	>0.4
Melt layer movement	>0.8	>0.6
Separate bridges	0.9-1.3 (after 50 pulses) 1.3-1.6 (after 10 pulses)	0.7-0.8 (after 100 pulses) 0.8-0.9 (after 50 pulses) 0.9-1.0 (after 20 pulses)
Surface melting	>0.9	>0.7
Gaps covering by melt material	1.3-1.6 (after 50 pulses)	0.8 (after 100 pulses) 0.9-1.0 (after 50 pulses)
Droplets ejection	>1.3	>1.0
Cracks formation	0.8-1.0 (type I and II) >1.0 (remelted)	>0.7 (remelted)
Boiling		>1.0 (near edges) >2.2 (intense)

It was also determined that the erosion processes of lanthanum tungsten start at the lower energy density as compared with pure tungsten. In other words the lanthanum tungsten erosion is higher than the erosion of pure tungsten at the same condition. (See Tab. 2, Fig. 2).

**Table 2.** Average erosion value  $\Delta h$ ,  $\mu\text{m}/\text{pulse}$

Q, MJ/m <sup>2</sup>	0.5	1.0	1.5	>2.2
PFCs				
W (>99,96%)	negligible	negligible	0.06	-
W-1%La <sub>2</sub> O <sub>3</sub>	0.005	0.04	-	3
CFC	negligible	negligible	0.3	3

At the energy density 1.0 MJ/m<sup>2</sup> the mass loss of pure tungsten was negligible but mass loss of the lanthanum tungsten sample corresponds to the specific erosion value 0.04 micrometers per pulse that is close to the value of the pure tungsten erosion at the energy 1.5 MJ/m<sup>2</sup>.

### 3. Droplet emission from W target.

Results of experimental and theoretical investigation of the droplet emission from W target under ELM-like plasma loads are presented in [6,11]. Onset condition of droplet production,

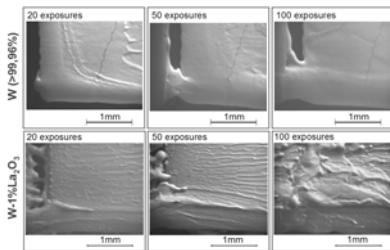


**FIG. 2** The view of the tungsten tile surface obtained by means of electron microscope.  $Q > 2.2 \text{ MJ/m}^2$

intensity of droplet ejection, velocities, and angular distributions of droplet ejection were studied on the flat tungsten target at QSPA-T facility. In the experiments target was oriented perpendicularly to the plasma flow in the first case and at 30 degrees in the second one. Statistical measurement of droplets characteristics has been performed at the absorbed energy density 1.6 MJ/m<sup>2</sup> with pulse duration of 0.5 ms for the normal plasma incidence.

Onset conditions of droplet ejection correspond to the absorbed energy density about 1.2 MJ/m<sup>2</sup> and the plasma pressure at the target surface about 1.8 atm. The mean droplet velocity is below 20 m/s. The main part of the emitted droplets has the velocity about 6 m/s. The 80% of the droplets are ejected at small angles to the target surface (less than 45°) Size of the measured droplets is equal to several tens of micrometers.

These experiments are supported by the numerical simulations. A rapid plasma flow along a thin melt layer film produces Kelvin-Helmholtz instability waves at the plasma-liquid

interface. Exponential growth of the KH waves leads to the wave breaking and droplet ejection. The calculations demonstrated a reasonable agreement with the experimental data on the droplet sizes and droplet velocities obtained in QSPA-T. Thus, the KH instability analysis carried out for the perpendicular plasma impact demonstrated: for  $Q > 1.3 \text{ MJ/m}^2$  the time of wave breaking is short enough to generate droplets. For the  $Q < 1.3 \text{ MJ/m}^2$  the time of wave breaking is rather long and droplet ejection would not be expected. The expected droplet sizes lie in the range 20-50  $\mu\text{m}$ , and velocities of the droplet ejection are in the range of 4-6 m/s. For the inclined plasma impact simulations demonstrated: the expected droplet sizes lie in the range 6-15  $\mu\text{m}$ , and expected velocities of the droplet ejection are in the range 10-20 m/s.

Numerical simulations carried out for heat loads anticipated after the ITER weak transients, in which plasma shielding does not occur, demonstrated the following. Plasma pressure at the target is much less than 0.2 bar (in QSPA-T - several bars), plasma density at the target surface is less than  $10^{-10} \text{ g/cm}^3$ , velocities of plasma flow are less than that being observed in the QSPA experiments. Thus for ITER weak transients the KH instability can not be generated during existing of the melt layer and droplet splashing would not be expected.

A rapid liquid motion in the melt layers along a convex edge of W-brush can generate the Rayleigh-Taylor instability which in the rotating rest-frame of the fluid is caused by the centrifugal acceleration in the melt layer. The RT instability can lead to the extension of the melt layer until the next macrobrush, thus producing the bridges between the brushes after the resolidification as it is seen in the experiments [5,6]. Also the droplets may form in perpendicular direction to the convex surface splashing into the plasma shield. Analysis of RT instability development carried out in [10] demonstrated that in case of violent melt motion with the melt velocity  $V_m = 1 \text{ m/s}$  the sharp edge leads to a fast growth of the RT instability and the droplet splashing can occur at the brush edges with  $R_{edge} < 0.001 \text{ cm}$ , with the drop size  $r_{RT} < 100 \mu\text{m}$ . In the opposite case the RT instability leads to the intense bridge formation between neighbour brushes, but a large radius of edge convex can prevent bridging. The dependences of critical edge convex radius preventing bridging as function of melt velocity are obtained.

#### 4. Cracking of tungsten under repetitive ELM-like loads.

The behavior of a preheated at 650 °C tungsten targets under repetitive ELM-like plasma pulses was studied in experimentally at the plasma gun QSPA Kh-50. [13,14]. The targets have been exposed up to 350 pulses of the duration 0.25 ms and the heat loads 0.45 MJ/m<sup>2</sup> and 0.75 MJ/m<sup>2</sup>, which is respectively below and above the melting threshold. It is shown that tungsten cracking can not be completely mitigated by the preheating above the DBTT, but it can be essentially minimized, especially below the melting threshold. Tungsten preheating above DBTT suppresses the macrocracks formation. After first hundred pulses only microcracks were found and it can be classified as fatigue cracks. Tungsten modification with

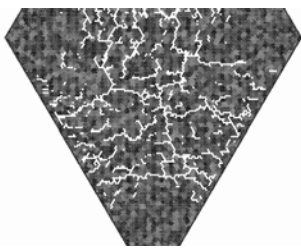


FIG. 3 PEGASUS-3D simulation of the cracks developed in tungsten sample after irradiation

formation of ordered submicron or nano-cellular structures in the surface layer was observed under irradiation with repetitive plasma pulses. The importance of cellular structures arisen for estimation of material response to the ITER transient events is demonstrated. For the preheated target with surface melting shots the tungsten damage by surface cracking became dominating after several hundreds of exposures similar to RT targets. The tungsten cracking is

accompanied by morphology evolution and by swelling of the surface demonstrating threshold dependence of the surface damage on the irradiation dose and influence of surface tension resulted in formation of “micro-brush” structures.

Numerical simulations of tungsten irradiation with hydrogen plasma in QSPA-Kh50 have been done using the PEGASUS-3D code [7]. It was found that the melting and the vaporization thresholds ( $0.56 \text{ MJ/m}^2$  and  $1.1 \text{ MJ/m}^2$ ) measured under the QSPA-Kh50 heating conditions for the undamaged tungsten samples are reproduced in the simulation. Numerical simulation of tungsten surface cracking under the thermostress in thin resolidified surface layer was also carried out. First results of simulation of the experiments qualitatively reproduce the crack pattern on the surface and its characteristic scales for plasma exposures with surface melting (See Fig. 3).

## 5. Numerical simulations of the CFC and W brush damage under ITER-like transients

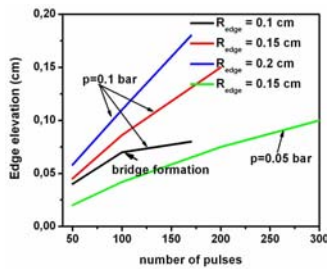


FIG. 4. Maximum mountain height vs pulse numbers.  $P$  pressure of the impacting plasma,  $R_{edge}$  – radius of brush edge rounding

damage were concentrated on investigation of repetitive heat load consequences [15]. The damage to W-macrobrush targets under repetitive ELM-like and disruptions heat loads corresponding to the conditions of the plasma gun QSPA-T and ITER is numerically

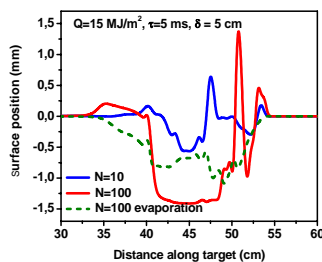


FIG. 5. Distribution of the erosion along the outer divertor after 10, and 100 disruption, SSP motion within  $\delta=5$

investigated with the three-dimensional melt motion code MEMOS in which changing of the surface roughness after previous transient was taken into account. The numerical simulations carried out for the QSPA-T repetitive heat loads demonstrated that the erosion monotonically increases with the number of ELMs. The melt mountain height is proportional to the ELM number (Fig. 4). The stochastic motion of SSP along the target surface significantly decreases the erosion due to melt motion and the vaporization in comparison with fixed SSP. This effect becomes significant as soon as the scanning width of stochastic motion twice exceeds the typical half-width of the surface roughness produced by single transient events. The repetitive disruptions will cause significant damages of the macrobrush target. For instance after 100 disruptions of the size  $15 \text{ MJ/m}^2$  and 5 ms a deep crater about 1.5 mm and a mountain near the crater edge of 1.5 mm appear (Fig. 5). For the bridge formation and the gap overlapping the centrifugal force at the brush edges is responsible. Bridge formation time depends on the brush edge rounding.

A comprehensive analysis of the numerical simulation results on CFC macrobrush damage under ITER-like transient heat loads as well as validation of the codes developed in FZK against QSPA-T experiments were done in [9]. Most important results were presented at IAEA FEC21. They may be written briefly as. Numerical simulations demonstrated that due to high heat conductivity pitch bundles sink mainly energy deposited at the target surface. That leads to the negligible erosion of pitch bundles and intense evaporation erosion of the PAN ones and lateral and frontal edges. Calculated dependences of PAN and pitch bundles erosion as functions of absorbed energy are in good agreement with measured (QSPA-T experiments) PAN bundle erosion.

**W-microbrush targets.** Numerical simulations of W brush damage were concentrated on investigation of repetitive heat load consequences [15]. The damage to W-macrobrush targets under repetitive ELM-like and disruptions heat loads corresponding to the conditions of the plasma gun QSPA-T and ITER is numerically investigated with the three-dimensional melt motion code MEMOS in which changing of the surface roughness after previous transient was taken into account. The numerical simulations carried out for the QSPA-T repetitive heat loads demonstrated that the erosion monotonically increases with the number of ELMs. The melt mountain height is proportional to the ELM number (Fig. 4). The stochastic motion of SSP along the target surface significantly decreases the erosion due to melt motion and the vaporization in comparison with fixed SSP. This effect becomes significant as soon as the scanning width of stochastic motion twice exceeds the typical half-width of the surface roughness produced by single transient events. The repetitive disruptions will cause significant damages of the macrobrush target. For

The calculations revealed a significant damage to brush edges caused by the interaction of impacting plasma with the lateral surfaces. In addition, experimentally observed overlapping of brush gaps by molten tungsten was numerically confirmed. These 3D effects of the repetitive transient loads may significantly influence the PFC lifetime.

## 6. Erosion simulation of Be armour.

The aim of the work presented in [12] is to provide reliable estimations of the damage to the Be-clad blanket modules under the Type I ELM and the disruption thermal quench loads (using the code MEMOS). The melting thresholds and melt layer depth of the Be armour under transient loads ( $Q = 0.2$  to  $2 \text{ MJ/m}^2$  and  $\tau = 0.2$  to  $0.6 \text{ ms}$ ) are estimated for different shapes of the transient. The results of numerical simulations of the erosion due to evaporation are also presented. The damage of FW under radiative heat arising during mitigated disruptions is estimated. The melt motion damages of Be macrobrush armour caused by the tangential friction force and the Lorentz force are analyzed for bulk Be and different sizes of Be-brushes. The damage of FW under radiative loads arising during mitigated disruptions is numerically simulated. Numerical simulation demonstrated that the velocity of melt motion and damage to the macrobrush targets with the sizes  $D \leq 2 \text{ cm}$  is significantly (by factor 4) less in comparison with that of bulk Be. The Lorentz force can generate violent melt motion that leads to the roughness formation exceeding ten  $\mu\text{m}$  per one ELM.

## 7. Conclusions.

PFC components manufactured according to the EU specifications for the ITER divertor targets, were exposed to ITER ELM-like ( $0.5 \text{ MJ/m}^2 < Q < 1.5 \text{ MJ/m}^2$ ) and disruption-like heat loads ( $Q > 2.2 \text{ MJ/m}^2$ ) in plasma gun facilities at TRINITI. The CFC erosion was mainly determined by PAN-bundles evaporation. Erosion was negligible at the energy density less than  $0.5 \text{ MJ/m}^2$ . The value of PAN-fibre erosion was in the range  $1.2 - 2.5 \mu\text{m/pulse}$  for ELM-like loads and increases up to  $6 \mu\text{m/pulse}$  for the disruption loads.

The tungsten erosion was mainly due to melt layer movement and droplets ejection. Erosion was negligible at the energy density less than  $0.5 \text{ MJ/m}^2$ . The noticeable erosion of tungsten was observed at the energy  $1.5 \text{ MJ/m}^2$  and average erosion calculated via mass losses was  $0.06 \mu\text{m}$  per shot. The significant erosion of the lanthanum tungsten started at the lower energy density. Erosion value of  $0.04 \mu\text{m}$  per shot was observed already at the  $1.0 \text{ MJ/m}^2$ . Onset conditions of droplets ejection from the pure tungsten surface correspond to  $1.2 \text{ MJ/m}^2$  of the adsorbed energy and  $1.8 \text{ atm}$  of the plasma pressure. The droplets velocities lie below  $20 \text{ m/s}$ . The effect of melt layer movement and droplets ejection in ITER may be less because the plasma pressure will be several times lower as compared with this experiments.

The measured material erosion data have been used to validate the codes, PEGASUS, MEMOS, PHERMOBRID and FOREV-2, which are further applied to model the erosion of the divertor and main chamber ITER PFCs under the expected loads in ITER. The numerical simulations of CFC damage under the QSPA conditions are in good qualitative and quantitative agreements with the experiments..

The numerical simulations carried out for the QSPA-T repetitive heat loads demonstrated that the erosion monotonically increases with the number of ELMs. The melt mountain height is proportional to the ELM number. For the bridge formation and the gap overlapping the centrifugal force at the brush edges is responsible. Bridge formation time depends on the

brush edge rounding. The numerical simulations for the ITER ELM-like repetitive heat loads with the expected plasma pressure below 0.1 bar demonstrated that in the case of brush edge radius larger than a critical radius the melt motion does not lead to the bridge formation.

The 3D MEMOS calculations revealed an additional significant damage to the brushes caused by the interaction of impacting plasma with the lateral surfaces. The simulation results on the damage under the repetitive heat loads are in rather good agreement with the QSPA-T experiments on W targets.

Melting thresholds and melt layer depth of the Be armour under transient loads are estimated for different temperatures of the bulk Be and different shapes of transient loads. The melt motion damages of Be macrobrush armour caused by the tangential friction force and the Lorentz force are analyzed for bulk Be and different sizes of Be-brushes. The damage of FW under radiative loads arising during mitigated disruptions is numerically simulated.

### Acknowledgement

This work, supported by the European Communities under the Contract TCN/350-02 of Association between EURATOM and Forschungszentrum Karlsruhe, was carried out within the framework of the European Fusion Development Agreement. The views and options expressed herein do not necessarily reflect those of the European Commission.

### References

- [1] ITER Physics Basis, Nucl. Fusion **39** (1999) 2137.
- [2] Federici, G., et al, Plasma Phys. Control. Fusion **45** (2003) 1523,
- [3] Loarte, A., et al., Physica Scripta T128 (2007) 222.
- [4] Loarte A., et al., Proc. 21<sup>st</sup> IAEA Conference, 2006, Chengdu, China.
- [5] Zhitlukhin, A., et al., J. Nucl. Mat. **363-365**, (2007) 301.
- [6] Klimov, N. et al. "Experimental study of PFCs erosion under ITER-like transient loads at plasma gun facility QSPA", 18<sup>th</sup> PSI Conference, Toledo Spain, May 2008, paper I-04
- [7] Pestchanyi S. and Linke J. Fusion Engineering and Design **82** (2007), 1657.
- [8] Pestchanyi S, 34<sup>th</sup> EPS Conference (EPS) Warsaw, Poland, 2-6 July 2007, paper D2.007.
- [9] Bazylev B., et al., Physica Scripta T128 (2007) 229.
- [10] Bazylev, B, et.al. Fusion Engineering and Design (2008), **In Press**
- [11] Bazylev, B. et al. "Experimental and theoretical investigation of droplet emission from tungsten melt layer" 25<sup>th</sup> SOFT, Rostock, Germany, September 2008. P1.59
- [12] Bazylev, B. et al. "Erosion simulation of first wall beryllium armour under ITER transient heat loads". 13<sup>rd</sup> ICFRM. December, 2007; Nice, France. To be published in the J. Nucl. Mat.
- [13] Makhlay, V., et al., Physica Scripta T128 (2007) 239.
- [14] Garkusha, I. et al., "Damage to preheated tungsten targets after multiple plasma impacts simulating ITER ELMs" 13<sup>rd</sup> ICFRM. December, 2007; Nice, France. To be published in the J. Nucl. Mat.
- [15] Bazylev, B. et al. "Experimental validation 3D simulations of tungsten melt erosion under ITER-like transient loads" 18<sup>th</sup> PSI Conference, Toledo Spain, May 2008, paper P1-87.